ARMA 12-667

Induced hydraulic fractures or reactivated natural fractures? Modeling the response of natural fracture networks to stimulation treatments

Williams-Stroud, S. C. and
Barker, W. B.,
MicroSeismic, Inc., Houston, TX, USA
Smith, K. L.
EnCana Oil & Gas (USA), Dallas, TX, USA

This paper was prepared for presentation at the 46th US Rock Mechanics / Geomechanics Symposium held in Chicago, IL, USA, 24-27 June 2012.

ABSTRACT: Microseismicity induced by hydraulic fracture stimulation of a horizontal well was mapped with a near-surface buried array. Distinct linear trends of events were not parallel to the direction of fast shear wave polarization measured in the reservoir with a crossed-dipole anisotropy tool. Analysis of core from a nearby well revealed numerous calcite-filled fractures that did not induce shear wave polarization, but did significantly impact the failure behavior of the reservoir rock during the stimulation treatment. Hydraulic fracture simulation with DFN modeling and source mechanism analysis supports the interpretation of reactivated existing fractures rather than the formation of hydraulically-induced tensile fractures.

1. INTRODUCTION

The development of linear trends of microseismicity during hydraulic fracture stimulation treatments has been typically interpreted to be indicators of the location of induced hydraulic fractures forming parallel to the maximum stress direction in the reservoir. Induced fractures failing in mode I tensile failure may not generate strong enough microseismic signal to be detected via microseismic monitoring methods, so often the microseismic events are interpreted to be the result of a shear failure "halo" around the hydraulic fracture or reactivation of intersecting natural fractures [1, 2]. Analysis of microseismic monitoring results acquired using an array of geophones buried in a grid over a wide area above the well allows collection of microseismicity without a directional bias [Fig 1.]. In addition, the wide aperture of the array provides coverage to detect signal at all azimuths so that it is possible to determine the full source mechanism for all events with sufficient energy detected by the array [3, 4].

We present a case study of a microseismic monitoring result that illustrates the significant impact that natural fractures in the reservoir can have on the stimulation. Source mechanism analysis shows that the failure planes of the events are parallel to the microseismic event trend, but the microseismic event trend is not parallel to the reservoir maximum horizontal stress interpreted from a crossed-dipole sonic log. Unoriented core taken from a nearby well contains numerous calcite filled fractures, which we interpret to have been exploited by the stimulation treatment. The directional trend of the micro-seismic events was used to infer the fracture orientation in the reservoir and to constrain to a discrete fracture network (DFN) model. Formation of hydraulic fractures was then simulated, using the hydraulic fracture treatment information in order to investigate the possible parameters leading to the observed event geometry. The results indicate that although hydraulic fractures can form in the reservoir, the great majority of the energy detected via microseismicity during the treatment occurred as a result of reactivation of the existing natural fracture network.

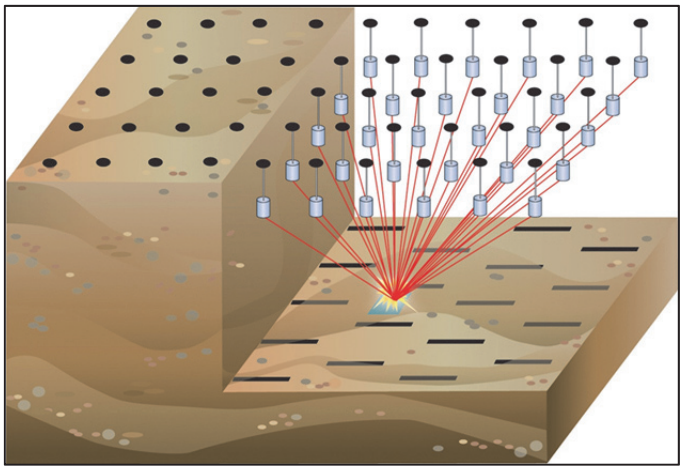

Figure 1. Schematic diagram of shallow buried geophone array detecting microseismic event in the subsurface.

2. CASE STUDY DESCRIPTION

Microseismic mapping of events induced during a hydraulic fracture stimulation treatment was done using a GSR recording system comprised of 98 geophones deployed at 300 feet below the surface above the monitoring area. Microseismic events induced by the hydraulic fracturing were located by a beam-forming process, which is essentially a one-way depth migration. The data quality was very good due to a low background noise level during the treatment so that it was possible to invert a large number of the events for their source mechanisms. A total of 108 hours of data were recorded, with 39 hours of data processed from 13 stages of stimulation treatments. Figure 2 shows a map view of the wellbore lateral and microseismic events detected by the monitoring array. The events are colored by treatment stage, and in most stages the length of the event trend indicating a fracture is at least 1000 feet on either side of the lateral. The beach ball representations of the source mechanisms determined from the largest events are displayed at their hypocenter locations for some of the largest amplitude events.

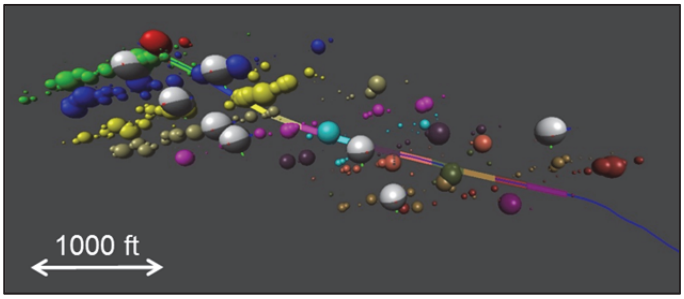

Fig. 2. Map view showing linear trends of microseismic events mapped during a well stimulation. Beach ball representations of source mechanism solutions for selected events are plotted at their hypocenter location. The bi-wing linear symmetrical pattern could be interpreted as indicating tensile fractures induced parallel to the maximum stress, but shear wave anisotropy analysis indicates S_{Hmax} is roughly perpendicular to the wellbore. Events are colored by stage and sized by energy.

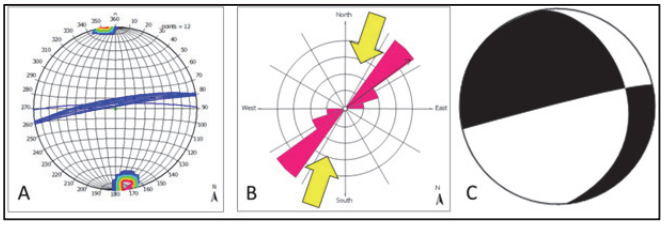

Fig. 3. (A) Stereonet plot of failure planes of 12 source mechanisms inverted from the induced microseismicity. The event trends indicate fracture growth of induced fractures is parallel to the source mechanism failure planes. (B) The direction of S_{Hmax} in the reservoir from anisotropy measured with crossed-dipole sonic log is shown by pink rose diagram with average S_{Hmax} orientation (yellow arrows) from the World Stress Map [5] The modeled hydraulic fractures have strike parallel to pink rose. (C) Beach ball representation of one of the source mechanisms.

All of the source mechanisms show a steeply dipping failure plane with oblique dip-slip displacement, which is consistent with an interpretation that S_{Hmax} is not parallel to one of the failure planes, and is also consistent with shear failure reactivation on an existing fracture plane (Fig 3). The anisotropy direction measured in the reservoir was interpreted to indicate the in-situ stress direction and not associated with fracture-induced anisotropy. Hydraulic fractures would be expected to form parallel to the maximum horizontal stress (parallel to the pink petals in the rose diagram in Figure 3); however, microseismicity trends did not develop in that orientation. Because the crossed-dipole sonic log only detected anisotropy from in-situ stress, fractures present in the reservoir were interpreted to be closed or healed during the acquisition of the sonic log, and so were invisible to the log. The interface between the reservoir rock and the calcite cement fill provided a preferential plane of weakness along which failure was induced during the treatment. A number of vertical calcite-filled fractures are clearly visible in vertical cores, indicating that these fractures are extremely common in this part of the reservoir (Fig. 4.)

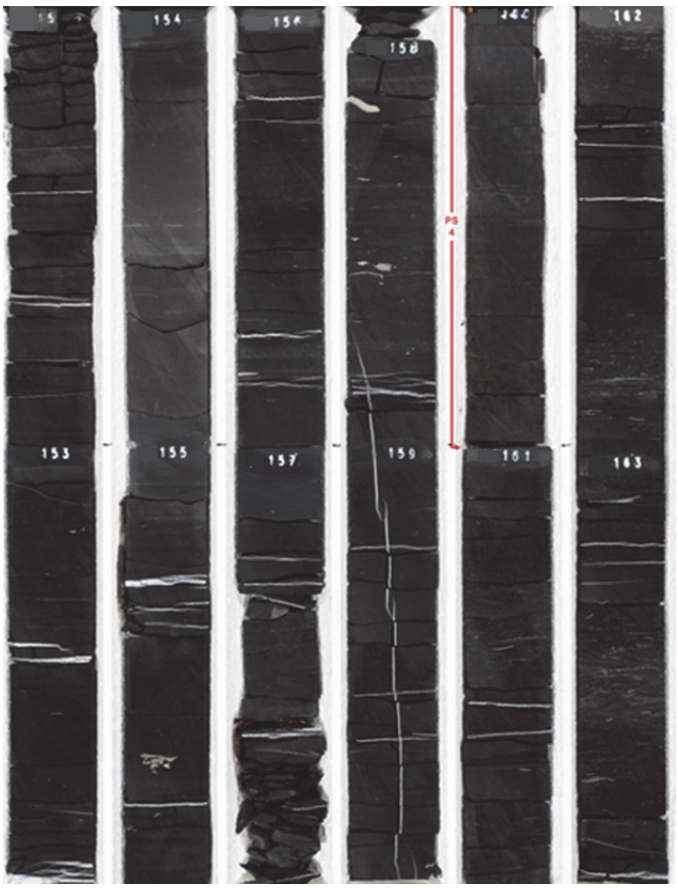

Fig. 4. Photograph of vertical core taken through the reservoir showing a sub-vertical calcite-filled natural fracture. The frequency of these fractures in the core is approximately every 6 meters (20 feet) indicating a relatively high fracture intensity in the reservoir, but they were invisible to the crossed-dipole sonic logging tool.

2.1. Implications of monitoring result

When source mechanism analysis is available from a treatment result the stress directions can be inferred from the failure planes of the microseismic events in the same way stress directions are inferred from natural earthquake focal mechanism solutions [6]. Analyses of source mechanisms of microseismic events can show that often the failure plane and microseismicity trends are not parallel, or that multiple source mechanisms occur during the same stimulation treatment [7]. Reactivation of larger failure planes, such as faults, reduces the effectiveness of the treatment, particularly when faults behave as a sink for fluid and proppant [8]. Treatments in which a large number of microseismic events were generated that are associated with reactivation of an existing fault can lead to poor production performance of the treated well. Conversely, reactivation of smaller discontinuities in fractured reservoirs is a desired outcome from the treatment when it induces complex failure on multiple fracture orientations [9, 10].

The microseismicity pattern mapped from the treatment of this well did not indicate complex failure, but rather mimics the appearance of induced tensile fractures. The initial production of this well suggests that reactivation of closed fractures during a stimulation treatment can expose sufficient reservoir surface area to effectively stimulate the well. Because the linear trends of the microseismic events suggest a lower amount of surface area was created during the hydraulic fracture treatment than would have been generated if a complex network of intersecting fractures were reactivated, the DFN modeling was undertaken to investigate the possible responses of the reservoir to the stimulation that might impact the resulting stimulated volume and permeability distribution.

3. FRACTURE MODELING METHODOLOGY

A DFN model was constructed using the well path and reservoir horizons. Logged bulk density to the surface was not available for this well, so an average density of 2.35g/cm^3 was assumed. The fracture orientations in the DFN were constrained by the orientation of the source mechanism failure planes, and multiple realizations of different fracture intensities were tested in order to find a fracture intensity where at least one natural fracture intersected the well bore at each of the 13 perforation stages. Figure 5 shows only the fractures that intersect the well bore from one of the DFN realizations with only the fractures that intersect the well bore displayed compared to the locations of detected microseismic events.

One fracture set was generated between the base of the reservoir and the top of one of the overlying units, as events were observed to occur above the reservoir interval. The fracture intensity measure type used was P32 (fracture area per unit volume of rock mass). Fracture sizes were constrained by an exponential length distribution with an equivalent fracture radius of 50 meters. The P32 value, 0.05, was chosen iteratively with different fracture size distributions by generating fracture sets with different combinations of P32 values and fracture length distributions until a result was derived with a sufficient number of fractures intersecting the wellbore.

Because the reservoir is relatively thin, the ratio of fracture length to height was set at 4:1 so fractures were less likely to extend above the reservoir. The mean principal orientation for the fracture set was taken directly from the failure plane orientations of the inverted source mechanisms.

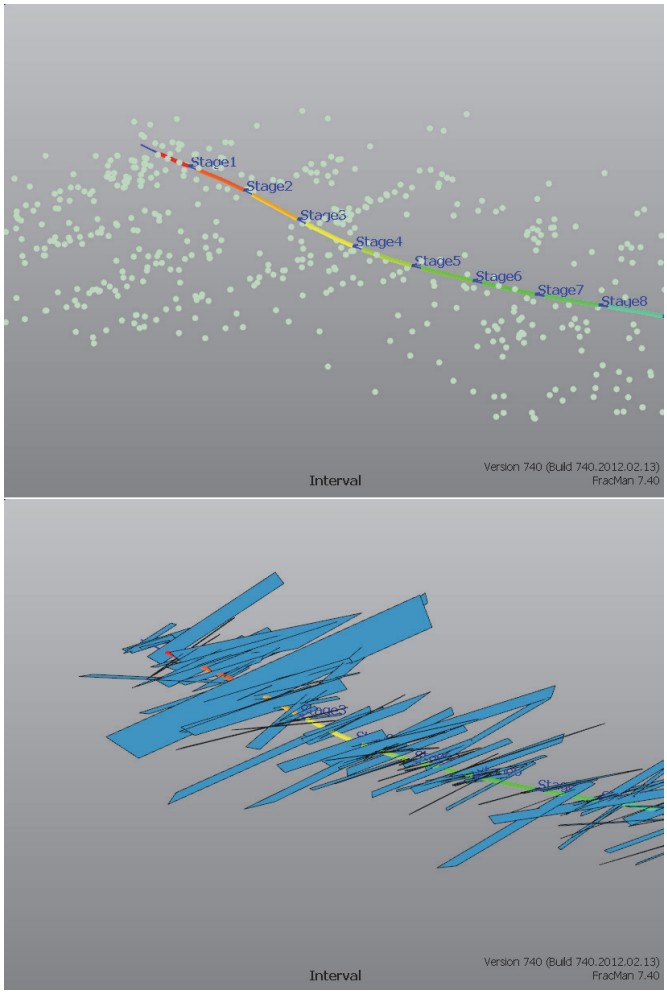

Fig 5. Horizontal wellbore showing stimulation intervals 1 through 8 and the microseismic events detected and located via monitoring during the treatment (top). The bottom image shows a subset of fractures from the DFN generated using the event source mechanism failure planes. Only the fractures in the DFN that intersect the well bore are displayed.

4. HYDRAULIC FRACTURE SIMULATION

The modeling approach requires a natural fracture network where the level of interaction with that fracture network is dependent on the in-situ stress field, the reservoir rock properties, the reservoir stresses and the treatment pressures and rates [11]. A hydraulic fracture develops from the wellbore parallel to the maximum horizontal stress direction in the model and any intersecting fractures are checked for a dilation criterion. If the normal stress on a fracture plane is less than the fracture pore pressure the fracture is considered dilatable, and slurry is pumped into that fracture. The total fracture volume of slurry received by the fractures in user-specified time steps contains both tensile hydraulic fractures and natural fractures that are dilatable at the end of a simulation run. Stimulation treatment volumes and rates for this well were used as the input parameters so that the calculated result provides a realistic possible fracture configuration that could contain all of the material pumped into the well during the treatment. The actual volume pumped into the well can serve as a calibration parameter for the hydraulic fracture simulation providing information for making model adjustments when the modeled volumes and the actual treatment volumes do not match.

We tested two different fracture stimulation interpretations:

- Stimulation by dilation of existing fractures that intersect the wellbore (Model 1)
- Stimulation by formation of new tensile fractures initiating at the wellbore (Model 2)

The same DFN representing the existing natural fracture network was used in both models. Table 1 shows a summary of the primary parameters that were varied in the two different models. All values were bracketed by the maximum stress, assumed to be vertical (calculated as described above in section 3) and the minimum stress which was based on the results of a DFIT (diagnostic fracture injection test) analysis from the well. Because information defining the full stress tensor was not available, a simple relationship for the principal stresses was chosen where stress anisotropy was defined by:

$$\sigma 3 = Pp + \frac{\sigma 1 - Pp}{3} \quad (1)$$

$$\sigma 2 = Pp + 2\left(\frac{\sigma 1 - Pp}{3}\right) \quad (2)$$

$$\sigma 1 = Pp + 3\left(\frac{\sigma 1 - Pp}{3}\right) \quad (3)$$

The pore pressure (Pp) can be estimated with drilling log correlations and the overburden can be calculated from the density log. For the modeling we assume a simple relationship for the stress distributions using the calculated overburden for this well where $Sv = \sigma_1$ and $Pp < \sigma_3 < \sigma_2 < \sigma_1$. Stress values were subdivided equally between the Pp and σ_1 by using the relationship in equations (1), (2), and (3) to create reasonable values to bracket possible stresses in the case where the actual σ_2 is not known. The hypothetical stress value calculated for σ_3 using this relationship is very close to the actual reservoir stress value calculated for pore pressure at closure from a DFIT test in the well.

One of the goals of the modeling was to test the assumption of new hydraulic fracture formation versus existing fracture reactivation. The input stresses were modified to preferentially generate hydraulic fractures by increasing the horizontal stress anisotropy. Because higher horizontal stress anisotropy and lower pumping pressure favors larger tensile fractures, the relative stress values were still bracketed by the Pp and σ_1, but slightly modified for Model 2. In order to optimize growth of the hydraulic fracture in the new tensile fracture mode, the stress anisotropy was increased by increasing the value of σ_2 as displayed in Figure 6. Pumping pressure for Model 2 was reduced to a value much closer to but still greater than σ_3.

4.1. Model 1 results

Hydraulic fractures generated in Model 1 are strongly dominated by the existing fracture network. Microseismic "events" generated at locations where failure occurs on fractures in the model form clouds with linear trends paralleling the fractures in the DFN (Fig. 7). Fracture stimulation starts as a hydraulic fracture that grows laterally away from the well bore at each stage, but which interacts with DFN fractures as it grows outward. The "events" colored by fracture stimulation stage also show interaction between different treatment stages.

Table 1. Summary of hydraulic fracture definitions and treatment pumping parameters

PARAMETER	MODEL 1	MODEL 2
Initiation	Intersecting fractures	New tensile fracture
Growth	Shear stress	N/A
Pump pressure/σ_1	0.947	0.933
Pump pressure/ σ_3	1.017	1.002
Pump duration (minutes)	120	120
Fracture flow priority	Fractures with higher permeability	Fractures parallel to maximum horizontal stress
Pump through non-dilatable fractures	No	yes

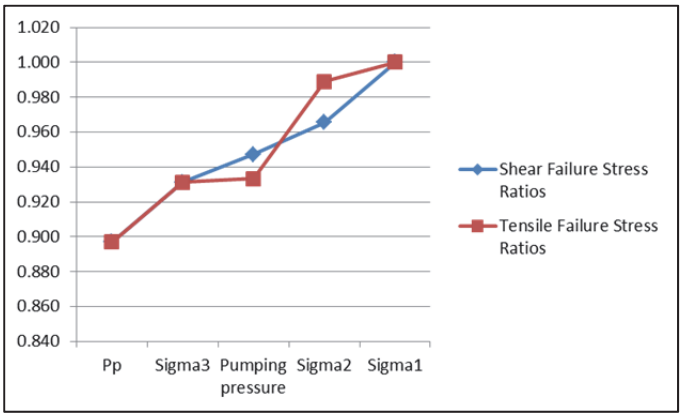

Fig. 6. Relationship of the modeled stress parameters used in hydraulic fracture simulation Model 1(hydraulic fractures forming from existing fractures and growth by shear failure – blue symbols) and Model 2 (hydraulic fractures initiating as new fractures at the wellbore – red symbols)

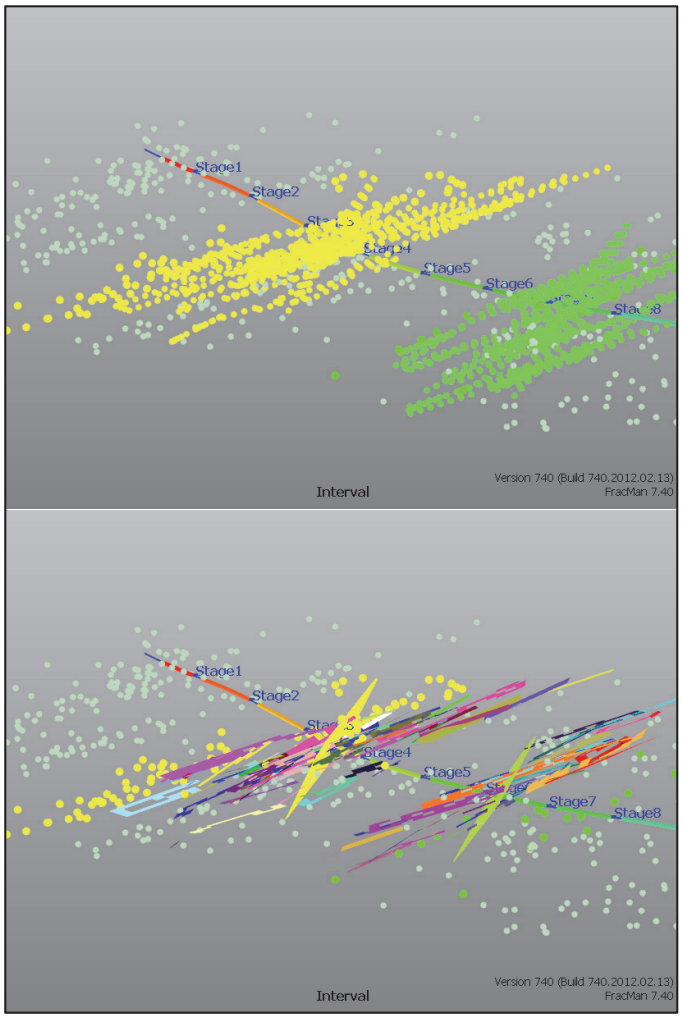

Fig 7. Microseismic "events" generated in Model 1 hydraulic fracture simulation showing the same trends as the strike of reservoir fractures for stage 4 and stage 7 and 8 (top). Fractures grow by shear failure according to the Mohr-Coulomb criterion after tensile failure first initiates in an existing fracture intersecting the wellbore (bottom).

4.2. Model 2 results

The impact of the existing DFN is minimal in the Model 2 simulation result. Given the same pumping rates, because the failure criterion is limited to tensile failure, very little failure occurs on the existing fractures, and the growing tensile fractures tend to terminate against them. The option to allow fluid to pump through non-dilatable fractures was chosen in order to allow fluid to contact more of the surface area in the existing DFN network. Fracture half-length did not extend beyond approximately 300 meters away from the wellbore for all of the model runs, and because the orientation of fractures in the existing network were not optimal for dilation, failure did not occur on them.

CONCLUSIONS

Modeling hydraulic fracturing in a reservoir as primarily reactivation of an existing fracture network resulted in a stimulated fracture network very similar to the microseismic mapping result presented in ~~a~~ this case study. Microseismic "events" generated from critically stressed points in the fracture network were compared to the distribution of actual microseismic events detected during the stimulation treatment by a shallow buried surface array. Dilation of tensile fractures generated in the model is calculated and a volume of slurry received by the tensile fractures can be validated by comparison to the actual volume of slurry pumped during the treatment. A volume of slurry received by the existing fracture network is also calculated and these fracture parameters can be used to provide a better constraint on fracture flow properties in DFNs generated for reservoir simulation modeling.

Finding the best fit model to the observed data provides a better understanding of the rock behavior during the treatment. The impact of natural fractures, reservoir stress, and treatment pumping parameters can be evaluated in order to predict the behavior of subsequent treatments in the same reservoir. Despite the development of the simple linear trends in this microseismic mapping result, the rock failure mode during the stimulation treatment appears to have been dominated by shear reactivation of existing fractures in the reservoir. The fact that this well is a strong producer supports the interpretation that shear failure on planes in an existing fracture network can be effective in exposing surface area of the rock to allow economic flow into the well.

ACKNOWLEDGEMENTS

The authors would like to thank EnCana Oil & Gas (USA) Inc., for permission to use the data and results in this paper.

REFERENCES

1. Rutledge, J.T., W.S. Phillips, and M.J. Maerhofer, 2004. Faulting induced by forced fluid injection and fluid flow forced by faulting: an interpretation of hydraulic-fracture microseismicity, Carthage Cotton Valley Gas Field, Texas. *Bull. Seismological Society of America.* 94:1817-1830.
2. Cipolla, C., X. Weng, M. Mack, U. Ganguly, H. Giu, O. Kresse, C. Cohen, and R. Wu. 2011. Integrating microseismic mapping and complex fracture modeling to characterize fracture complexity, SPE 140185
3. Williams-Stroud, S., J. E. Kilpatrick, B. Cornette, L. Eisner, M. Hall, 2010. Moving outside of the borehole: characterizing natural fractures through microseismic monitoring. *First Break*, 28:89-94.
4. Wessels, S. A., A. De La Pena, M. Kratz, S. Williams-Stroud, T. Jbeili, 2011. Identifying faults and fractures in unconventional reservoirs through microseismic monitoring. *First Break*, 29:99-104
5. Heidbach, O., M. Tingay, A. Barth, J. Reinecker, D. Kurfeß, B. Müller, 2009. The World Stress Map based on the database release 2008, equatorial scale 1:46,000,000, *Commission for the Geological Map of the World*, Paris, doi:10.1594/GFZ.WSM.Map2009.
6. Aki, K., and P. G. Richards, 2002, *Quantitative Seismology*, University Science Books, Sausalito, CA.
7. Williams-Stroud, C., and L. Eisner, 2010. Stimulated fractured reservoir DFN models calibrated with microseismic source mechanisms. ARMA 10-520.
8. Hulsey, B.J., B. Cornette, D. Pratt, 2010. Surface microseismic mapping reveals details of the Marcellus Shale, SPE 138806-PP.
9. Fisher, M.K., J.R. Heinze, C.D. Harris, B.M. Davidson, C.A. Wright and K.P. Dunn, 2004. Optimizing horizontal completion techniques in the Barnett Shale using microseismic fracture mapping. SPE 90051
10. Wu, R., O. Kresse, X. Wang, C. Cohen, and H. Gu, 2012, Modeling interaction of hydraulic fractures in complex fracture networks. SPE 152052
11. Dershowitz, B., LaPointe, P., Eiben, T., Wei, L., 2000, Integration of discrete feature network methods with conventional simulator approaches, *SPE Reservoir Evaluation and Engineering*. 3:165-170